Original Article
Effect of subcutaneous adipose tissue-associated CSRP2 on the progression of prostate cancer via the WDR5/USP44 pathway

Juan Wang[1,2*], Yuting Liang[3*], Kaiwen Wang[4], Lihui Lin[1,2], Xia Peng[1,2], Weize Li[1,2], Yanning Li[1,2], Huanjin Liao[1,2], Jia Li[5], Longwei Qiao[6], Li Li[1,2]

[1]Department of Laboratory Medicine, Shanghai General Hospital, Shanghai Jiao Tong University School of Medicine, Shanghai, China; [2]College of Health Science and Technology, Shanghai Jiao Tong University School of Medicine, Shanghai, China; [3]Center for Clinical Laboratory, The First Affiliated Hospital of Soochow University, Suzhou, Jiangsu, China; [4]Department of Rheumatology, Shanghai Renji Hospital, Shanghai Jiao Tong University School of Medicine, Shanghai, China; [5]Medical Laboratory, Shidong Hospital Affiliated to University of Shanghai for Science and Technology, Shanghai, China; [6]Center for Reproduction and Genetics, School of Gusu, The Affiliated Suzhou Hospital of Nanjing Medical University, Suzhou Municipal Hospital, Nanjing Medical University, Suzhou, Jiangsu, China. *Equal contributors.

Abstract: Elevated subcutaneous adipose tissue in obese men correlates strongly with a higher risk of aggressive prostate cancer and poor treatment outcomes, but the exact mechanism underlying the increased risk remains elusive. To address this question, we analyzed prostate cancer transcriptomic data from The Cancer Genome Atlas as well as single-cell RNA sequencing and tissue microarray data from prostate cancer cells. Subcutaneous adipose tissue-associated cysteine-rich protein 2 (CSRP2) was significantly downregulated in prostate cancer epithelial cells. Knockdown of CSRP2 promoted proliferation of prostate cancer cell lines DU145 and PC3, whereas the opposite effect was observed with CSRP2 overexpression. *In vivo* xenograft assays confirmed that CSRP2 overexpression inhibits the growth of prostate cancer cells. Importantly, co-immunoprecipitation and mass spectrometry assays confirmed that CSRP2 inhibits the deubiquitination of WD40 repeat protein 5 (WDR5) by ubiquitin-specific protease 44 (USP44). Overexpression of WDR5 reversed the growth inhibition of CSRP2 overexpression on prostate cancer cells. Altogether, our data indicate that CSRP2 suppresses prostate cancer cell proliferation via a CSRP2/WDR5/USP44 dependent pathway to control prostate cancer progression, suggesting a potential mechanism for prostate cancer treatment.

Keywords: Prostate cancer, subcutaneous adipose tissue, CSRP2, WDR5

Introduction

Prostate cancer, the second leading cause of cancer-related death among males, is characterized by significant heterogeneity and highly variable prognosis outcomes [1]. Local treatment such as laparoscopic radical prostatectomy results in a 10-year survival rate > 99% in approximately 80% of men diagnosed with prostate cancer [2, 3]. However, approximately 5% of prostate cancer patients develop distant metastases at one or more sites and 15% develop local metastatic cancer [2]. Ultimately, nearly all patients who develop metastatic prostate cancer progress to castration-resis-

tant prostate cancer [4]. This diversity in prognosis is likely associated with tumor heterogeneity [5]. Limited prostate cancer comprises multiple tumor foci, each of which exhibits unique molecular characteristics as well as variable potential for metastasis and susceptibility to treatment [6, 7]. Therefore, to improve patient outcomes, there is an urgent need to identify and characterize the cellular signaling pathways that can delay or inhibit prostate cancer progression and improve the efficacy of therapy.

Previous studies identified obesity as a risk factor for several chronic diseases including hyper-

tension, dyslipidemia, type 2 diabetes [8], and postmenopausal breast, prostate, endometrial, pancreatic, and thyroid cancers. Notably, obesity strongly influences the risk and progression of prostate cancer [8, 9] while obese male cancer patients with abundant subcutaneous adipose tissue develop more aggressive forms of cancer and exhibit worse treatment outcomes, an elevated risk of biochemical recurrence (BCR) after radical prostatectomy, and higher cancer-specific mortality [10-12]. Mechanistic studies have explored whether factors such as leptin, altered inflammatory profile, chronic hyperinsulinemia, or dyslipidemia increase cancer risk in obese males [13, 14]. It has been proposed that an altered leptin/lipocalin ratio in obese individuals leads to altered AMPK/mTOR signaling which in turn increases prostate cancer risk [13]. Alternatively, obesity-associated low levels of insulin-like growth factor-binding protein (IGF-BP) could lead to increased stimulation of insulin-like growth factor-1 (IGF-1) and its downstream effectors including the phosphatidylinositol-3 kinase (PI3K)/Akt/mTOR pathway [14]. Nevertheless, the mechanism by which obesity and increased subcutaneous adipose tissue increase prostate cancer risk remains poorly understood.

The present study explores the role of factors associated with subcutaneous adipose tissue in promoting prostate cancer progression with special emphasis on CSRP2. Data resources used in this study included previously reported RNA-seq and single-cell (sc) RNA-seq datasets and these were combined with *in vitro* cell-based assays and an *in vivo* xenograft tumor assay using nude mice. Initially, a subcutaneous adipose tissue gene expression signature was derived via bioinformatic analyses of RNA-seq data. Subsequent analysis of The Cancer Genome Atlas (TCGA) data on overall survival (OS) of prostate cancer patients identified 10 key marker genes differentially expressed in subcutaneous adipose tissue. Noting significant downregulation of CSRP2 in both prostate cancer and pan-cancer contexts, a prognostic model was developed and used to explore the significance of the proposed critical prostate cancer marker genes as determinants of prostate cancer prognosis, tumor microenvironment (TME) infiltration, immune escape, and chemotherapeutic response. The downregulation of CSRP2 in tumor cells was further vali-

dated using scRNA-seq data and tissue microarrays. The effects of CSRP2 knockdown and overexpression in two prostate cancer cell lines were also examined *in vitro* and *in vivo*. Finally, candidate protein-interacting partners of CSRP2 were identified using co-immunoprecipitation (Co-IP) and mass spectrometry (MS). Together, the data presented here suggest that CSRP2 is a critical negative regulator of prostate cancer progression whose downstream effectors include the deubiquitinating enzyme USP44 and the WDR5 oncogene. The results provide a new perspective on the prognostic assessment of prostate cancer and could potentially lead to novel therapeutic interventions that prevent or delay prostate cancer progression.

Materials and methods

Building a model for prostate cancer based on subcutaneous adipose tissue-associated differentially expressed genes

Differentially expressed genes associated with subcutaneous adipose tissue were identified in the GSE24883 dataset [15] using *p*-value < 0.05 and |log2FC| > 0.5 as selection criteria. Subsequently, prostate cancer patient RNA-seq data and clinical information from TCGA database were subject to univariate Cox survival analysis to identify genes associated with OS from prostate cancer. To enhance prediction accuracy, least absolute shrinkage and selection operator (LASSO) regression analysis was used to identify 10 genes critical for prostate cancer risk and these genes were used to develop a prostate cancer risk model. TCGA prostate cancer patients were stratified into high-risk and low-risk groups based on the median value derived from the risk score. To evaluate the prognostic predictive reliability of the risk-scoring system, Kaplan-Meier analysis was performed. Progression-free survival interval and time-dependent receiver operating characteristic curves were generated and plotted using "survivalROC" from the R software package.

From TCGA, we obtained differential gene expression analysis in the model and analyzed copy number variation and somatic mutations. The expression of CSRP2 in pan-cancer was investigated using TCGA and Genotypic Tissue Expression (GTEx) data.

Prognosis-related pathways and tumor micro-environment

To explore prognostically relevant signaling pathways, we applied the "clusterProfiler" software package and performed Gene Ontology (GO), gene set variation (GSVA), and Kyoto Encyclopedia of Genes (KEGG) analyses. The Mutation Annotation Format was extracted from the TCGA data using the "maftools" R package to identify mutations linked to different prostate cancer risk-scoring groups. The relationships between the proportion of 20 infiltrating immune cells, the 10 characterized genes, and risk scores were explored using CIBERSORT. The R package "estimate" and gene expression profiles were used to infer the abundance of mesenchymal and immune cells and tumor size. "pRRophetic" was used to maximize the potential of the model to predict outcomes of targeted chemotherapy; specifically, the IC_{50} was calculated for two classical chemotherapeutic agents used to treat prostate cancer.

Analysis of single-cell RNA sequencing data

scRNA-seq data from tumor and prostate biopsies were obtained from the GSE176031 dataset and analyzed using the "Seurat" package [16]. Data were excluded from the analysis if the percentage of mitochondrial genes exceeded 20% and if < 200 or > 10000 genes were expressed in the source cells. Gene expression data were normalized using the "NormalizeData" function of the software. Principal component analysis was performed and the first 19 PCs based on the first 2000 highly variable genes were identified. Marker genes for each cluster were identified using the "FindAllMarkers" function and cell types were annotated using the "SingleR" package.

CSRP2 expression was analyzed in various cell and disease subpopulations and represented graphically using violin and UMAP plots. Furthermore, cell populations were stratified into high- and low-expression subgroups based on the median CSRP2 expression in epithelial cells. Differentially expressed genes were identified using the Wilcoxon rank-sum test. Functional enrichment for differentially expressed genes was assessed using single-sample gene set expression analysis. In addition, "pseudotime" and the Monocle algorithm were used to analyse CSRP2 expression in epithelial cells. Downscaling analyses were executed for each cell subpopulation using the DDR Tree algorithm. The resulting "plot_pseudotime_heatmap" was used to graphically represent differential gene modules that covary along pseudotime.

Cell culture and transfection

PC3 and DU145 human prostate cancer cell lines were acquired from Cyagen Biosciences (Guangzhou, China) and cultured in RPMI-1640 medium (Gibco, CA, USA) supplemented with 10% fetal bovine serum. The cells were cultured at 37°C in a humidified incubator with 5% CO_2. For transient knockdown of CSRP2, si-CSRP2 was transfected into PC3 and DU145 cells using Lipofectamine 2000 (Invitrogen, USA), following the manufacturer's instructions. si-CSRP2 was composed of the following ssRNA oligomers: si-CSRP2-1, sense 5' GAAGAGAUC-UACUGCAAAU(dT)(dT)-3' and antisense AUUU-GCAGUAGAUCUCUUC(dT)(dT); si-CSRP2-2, sense 5' CAGGCCUACAACAAAUCCA(dT)(dT)-3' and antisense UGGAUUUGUUGUAGGCCUG(dT)(dT). Lipofectamine 2000 (Invitrogen, USA) was used to transfect OV-CSRP2 (pcDNA3.1-CS-RP2), pcDNA-WDR5, and empty vector (Gene-Pharma, Suzhou, China) into cells overexpressing CSRP2 and WDR5. Cells were harvested 48 h post-transfection.

RNA extraction and RT-qPCR

Total RNA was extracted from PC3 and DU145 cells using Trizol and mRNA was reverse transcribed using the PrimeScript Reverse Transcription Kit (Vazyme, Nanjing, China). mRNA expression was quantified using the ABI 7500 Real-Time PCR system (Applied Biosystems, Inc., Foster City, CA, USA) and SYBR qPCR SuperMix Plus (Novoprotein Scientific Co., Ltd., China). 18S rRNA was used as an internal control and relative expression was calculated using the 2-ΔΔCt method. RT-qPCR reactions were conducted using the following primers: CSRP2 forward 5'-TATGGGCCAAAAGGCTACGG-3' and reverse 5'-CAGGGCTTTCCAGCTCCAAT-3', 18S rRNA forward 5'-CCTCCAATGGGATCCTCG-TTA-3' and reverse 5'-AAACGGCTACCACATCCA-AG-3'.

Tumor biological behavior assay

Cell viability was assessed using a CCK-8 kit (Beyotime, Beijing, China). Assays were per-

formed in 96-well plates inoculated with 5000 cells per well. Cells were incubated with 10% CCK-8 medium for 1 h at 24 h intervals. Cell number was determined by measuring optical density at 450 nm using a microplate reader (Geneomaga).

After transfection, prostate cancer cells were seeded in 6-well plates at 500 cells per well and cultured for 2 weeks. Culture medium was renewed every three days. Cells were washed twice with ice-cold phosphate-buffered saline, fixed in 4% paraformaldehyde for 30 min, and stained with 1% crystal violet for 30 min. Stained cells were photographed and cell numbers were determined using ImageJ software.

After knockdown or overexpression, aliquots of 100 μl were seeded on transwell plates. Culture medium containing 10% FBS was placed in the lower chamber and cells were incubated for 48 h. Unmigrated cells were gently removed with a sterile cotton swab, while migrated cells were fixed on the lower side in 4% paraformaldehyde, stained with 1% crystal violet for 40 min, and visualized under an inverted microscope. At least three fields were selected at random and photographed.

Xenograft assay

Prostate cancer cell growth was analyzed *in vivo* as follows. Prostate cancer cells were transfected with a CSRP2 expression plasmid or a control plasmid. Subsequently, 5×10^6 transfected cells were injected subcutaneously into the left ventral dorsum of each male BALB/c nude mouse. Tumor volume and weight were measured every 3 days, and tumor cell proliferation was assessed by immunofluorescence. The method of euthanasia for mice used in research is CO_2 inhalation. Prior approval was obtained from the ethics committee of the host institution.

Immunofluorescence

5 μm sections were prepared from paraffin-embedded prostate cancer and control xenograft cells or prostate cancer tissue and para-cancerous tissue. The sections were incubated overnight at 4°C with 100 μl of primary antibody (anti-Ki67, anti-CSRP2, Proteintech) diluted in 5% bovine serum albumin. Alexa Fluor was used as secondary antibody and sections

were stained with 4',6-diamidino-2-phenylin-dole (DAPI) and visualized under a confocal laser microscope.

Immunoprecipitation (IP) assay

Co-IP assays were conducted using cell lysates and anti-CSRP2-flag antibody (Sigma, F1804), anti-WDR5-GFP antibody (Santa, SC-9996), or anti-USP44-HA antibody (Santa, SC-7392). Cells were lysed by incubation in RIPA lysis buffer (Beyotime, Nantong, China) on ice for 30 min, then incubated with 20 μL washed beads carrying the corresponding antibodies (Sigma, USA) for 2 h at 4°C. The beads were transferred to sample buffer and heated at 100°C for 10 min. Beads were separated from the supernatant, which was analyzed by gel electrophoresis, protein blotting, and liquid chromatography-tandem mass spectrometry (LC-MS/MS).

Liquid chromatography-mass spectrometry analysis

Gel pellets containing proteins of interest were washed sequentially with deionized water followed by 50% and then 100% acetonitrile. Subsequently, the sample was reduced and then alkylated for 45 min at room temperature, washed thoroughly, and gently air-dried. The samples were hydrogelized for 30 minutes at 4°C, followed by a 12-hour digestion at 37°C. All resulting extracts and supernatants were combined and dried using a SpeedVac. The digested peptides were desalted using a StageTip and analyzed using an LTQ Orbitrap-Velos mass spectrometer. Tandem mass spectra were obtained and used as queries to search the UniProt protein database for matching proteins and peptides. The false discovery rate was set to 1%. All experiments were conducted in triplicate, and protein expression levels were estimated using the iBAQ algorithm integrated into MaxQuant for label-free quantification.

Western blot analysis

Cells were lysed in RIPA buffer and cellular proteins were extracted from the cell lysates. Aliquots containing equal amounts of total cellular protein were electrophoretically separated on 10% sodium dodecyl sulfate-polyacrylamide (SDS-PAGE) gels and transferred to PVDF membranes (Bio-Rad, Hercules, CA, USA). GAPDH

(cat. no. 60004; 1:1000; Proteintech) and anti-WDR5 (cat. no. 15544; 1:1000; Proteintech) were used as primary antibodies. The membranes were incubated with an HRP-coupled secondary antibody (cat. no. SA00001-2; 1:1000; ProteinTech) for 1 h at room temperature and protein bands were detected using a chemiluminescence kit (Beyotime, Shanghai, China).

Protein half-life assay

Aliquots of prostate cancer cells were treated with cycloheximide (100 μg/mL) at time points (0, 3, and 6 h) after transfection with pcDNA3.1 or pcDNA3.1-CSRP2. Proteins were harvested from the cycloheximide-treated cells and analyzed by SDS-PAGE followed by Western blot using an antibody to WDR5.

Statistical analysis

Statistical analysis was performed using GraphPad Prism 9.0 (GraphPad Inc., USA) or R. A minimum of three independent replicate experiments were performed. Results are presented as the mean ± standard deviation (SD). Differences between two or more groups were evaluated for statistical significance using Student's t-test or one-way ANOVA analysis. Statistical significance thresholds were $*P < 0.05$, $**P < 0.01$, $***P < 0.001$.

Results

Identification of subcutaneous adipose tissue-associated differentially expressed genes including CSRP2 and development of a prognostic model for prostate cancer

An initial search for genes that are differentially expressed in subcutaneous adipose tissue identified 1394 candidate genes using the previously published GSE24883 dataset [15] with a *p*-value cutoff of < 0.05 and |log2FC| > 0.5 (**Figure 1A**). Subsequently, a univariate Cox survival analysis was performed to identify 661 genes associated with OS in patients with prostate cancer. Venn diagrams were used to identify 34 genes that are differentially expressed in subcutaneous adipose tissue and associated with OS in prostate cancer patients (**Figure 1B**). Subsequent LASSO analysis of these 34 genes identified the following ten genes of interest: *TACC3, CCNL2, GPR35, CSRP2,*

PAQR6, E2F1, LY6G5B, SVOPL, NEK3, and *DRD5* (**Figure 1C-E**). Prostate cancer risk models based on these 10 genes were then constructed and the model was used to stratify prostate cancer patients into high- and low-risk groups based on their predicted risk score. **Figure 1** shows that patients classified by the model as high-risk exhibited notably worse outcomes (*i.e.*, shorter progression-free survival interval) than patients classified as low-risk (**Figure 1F, 1G**). Receiver operating characteristic curves showed 1-, 3-, and 5-year AUCs of 0.820, 0.788, and 0.728, respectively (**Figure 1H**). These analyses demonstrate the reliability of the risk prediction model for prostate cancer.

To identify biological processes that could modulate prostate cancer risk, GO and KEGG enrichment analyses were performed. GO analysis indicated significant enrichment in ubiquitin-like protein ligase binding and ubiquitin-protein ligase binding (Supplementary Figure 1A). Furthermore, GSVA of KEGG terms revealed that enrichment in pathways related to base excision repair, homologous recombination, and DNA replication correlated with high prostate cancer risk, while enrichment in pathways related to butanoate metabolism, propanoate metabolism, valine, leucine, and isoleucine degradation, and fatty acid metabolism correlated with low prostate cancer risk (Supplementary Figure 1B). Supplementary Figure 1C illustrates the mutational landscape associated with low and high prostate cancer risk and reveals significantly more mutations in the high-risk group. Infiltration of immune cells and expression of the 10 marker genes identified above (**Figure 1C-E**) were also examined in high and low-risk groups. It is noteworthy that resting CD4 memory T cells and resting mast cells were negatively correlated with prostate cancer risk, whereas T cell regulation and T follicular helper cells were positively correlated with prostate cancer risk (Supplementary Figure 1D). In addition, it is worth noting that the correlation between CSRP2 and immune cells is relatively modest. The immune score and ESTIMATE score in the tumor microenvironment score were also significantly higher in the high-risk group (Supplementary Figure 1E).

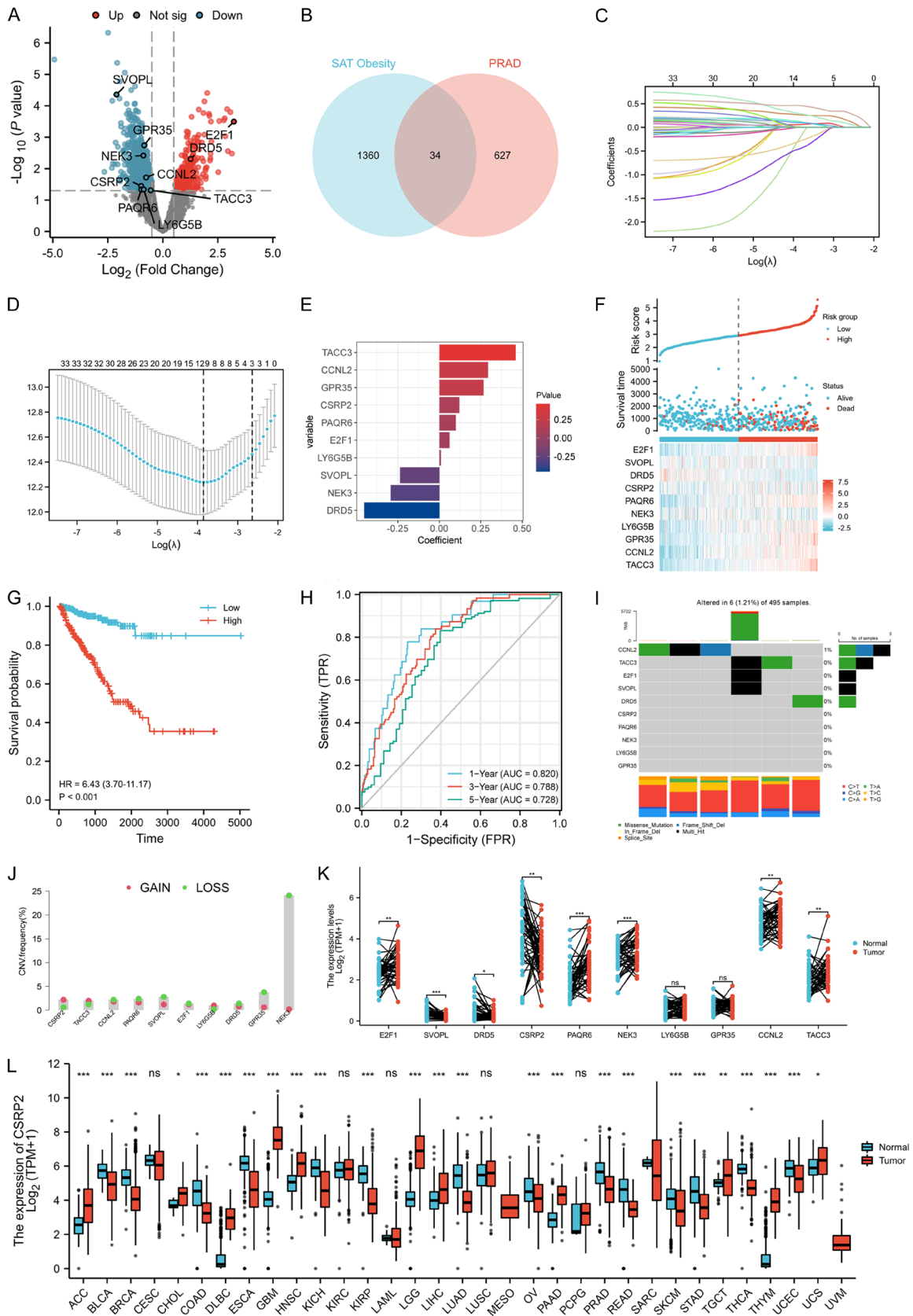The relationship between prostate cancer risk score and tumor stemness was evaluated using

Figure 1. Construction of a model based on subcutaneous adipose tissue-associated genes including CSRP2. A. The volcano map depicts subcutaneous adipose tissue characteristic genes differentially expressed in thin and obese

people from the GSE24883 dataset. B. Venn diagrams showed 34 genes associated with subcutaneous adipose tissue and prostate cancer OS. C-E. LASSO analysis identified 10 key genes subsequently used to construct a prostate cancer prognostic model. F. Risk score (up) and hot maps (down) of key gene expression in prostate cancer patients G. The progression-free interval (PFI) of high-risk patients and low-risk patients. H. ROC curves of the model predict OS1-, 3-, and 5-years of prostate cancer patients. I. Incidence of TMB in 495 patients with prostate cancer. J. CNV analysis revealed genes with large copy number variations. K. Differential analysis of model genes using TCGA data from paired prostate cancer samples. L. Pan-cancer analysis of CSRP2 expression in TCGA and GTEx datasets.

RNA stemness score (RNAss). The results showed a significant positive correlation between prostate cancer risk score and tumor stemness (Supplementary Figure 1F). The usefulness of the model for predicting the response to chemotherapy was also explored. Notably, patients in the high-risk group exhibited greater sensitivity to cisplatin and were insensitive to the androgen receptor blocker bicalutamide (Supplementary Figure 1G).

Furthermore, somatic mutations in the 10 prostate cancer marker genes were identified and evaluated (**Figure 1I** and Supplementary Figure 1B, where 1.21% of the samples carried mutations). This analysis revealed higher copy number variation at *NEK3* and *GPR35* (**Figure 1J**). Based on TCGA data, the expression of *E2F1*, *PAQR6, NEK3, CCNL2*, and *TACC3* was higher and upregulated in prostate cancer, while expression of *CSRP2* was downregulated (**Figure 1K**). Data from TCGA and GTEx showed that CSRP2 was significantly downregulated in prostate cancer and other sex-related cancers including breast (BRCA) and ovarian cancer (OV), and uterine corpus endometrial carcinoma (UCEC) (**Figure 1L**). From ten characteristic genes, *CSRP2* was identified as the only significantly downregulated gene that had not yet been thoroughly investigated in the context of prostate cancer. Given that the function and mechanism of CSRP2 in prostate cancer remain unclear, it was chosen as the target molecule for in-depth study.

Downregulation of CSRP2 detected by scRNA-seq analysis of prostate cancer cells

To better understand the expression of CSRP2 in the prostate cancer cell microenvironment, the scRNA-seq dataset GSE176031 was analyzed. GSE176031 includes data from 17 tumor samples and 10 normal samples. Following rigorous quality control procedures, data from 18,198 high-quality cells (11,429 tumor-derived and 6,769 normal cell-derived) were selected for analysis. Employing the UMAP visu-

alization technique, 19 clusters were selected using downscaled clustering of all cells (**Figure 2A**). Utilizing the "SingleR" software package, seven cell clusters were discerned based on marker genes, namely T cells, epithelial cells, monocytes, endothelial cells, smooth muscle cells, NK cells, and B cells (**Figure 2B**). Notably, within clusters 1, 3, 7, 8, and 15, epithelial cells exhibited higher expression of CSRP2, prompting us to designate them as "CSRP2 epithelial cells" (**Figure 2C**). Remarkably, high expression of CSRP2 was detected in epithelial, endothelial, and smooth muscle cells, while negligible CSRP2 expression was detected in immune cells (**Figure 2D**). However, CSRP2 expression was markedly lower in tumor-derived epithelial cells than in normal tissue-derived epithelial cells (**Figure 2E**).

To identify and understand the functions and pathways associated with high expression of CSRP2 in epithelial cells, we first identified 1 378 genes whose expression correlated with expression of CSRP2 (Supplementary Figure 2A) and then analyzed the functions of these genes using "FindAllMarkers" and the Wilcoxon test. This analysis revealed that these genes were predominantly enriched in cellular responses to stress, protein processing in the endoplasmic reticulum, intracellular protein transport, organization of the endomembrane system, cellular homeostasis, response to endoplasmic reticulum stress, and positive regulation of protein localization.

CSRP2-expressing epithelial cells were also stratified into high- and low-expressing groups based on the mean value of CSRP2 expression (Supplementary Figure 2B, 2C), and showed that high CSRP2-expressing epithelial cells were more abundant in normal tissue than in prostate cancer tissue. This suggests a pivotal role for CSRP2-overexpressing epithelial cells in prostate cancer progression. "FindAllMarkers" and the Wilcoxon test were then used to identify 209 genes that were differentially expressed in CSRP2 high- and low-expressing
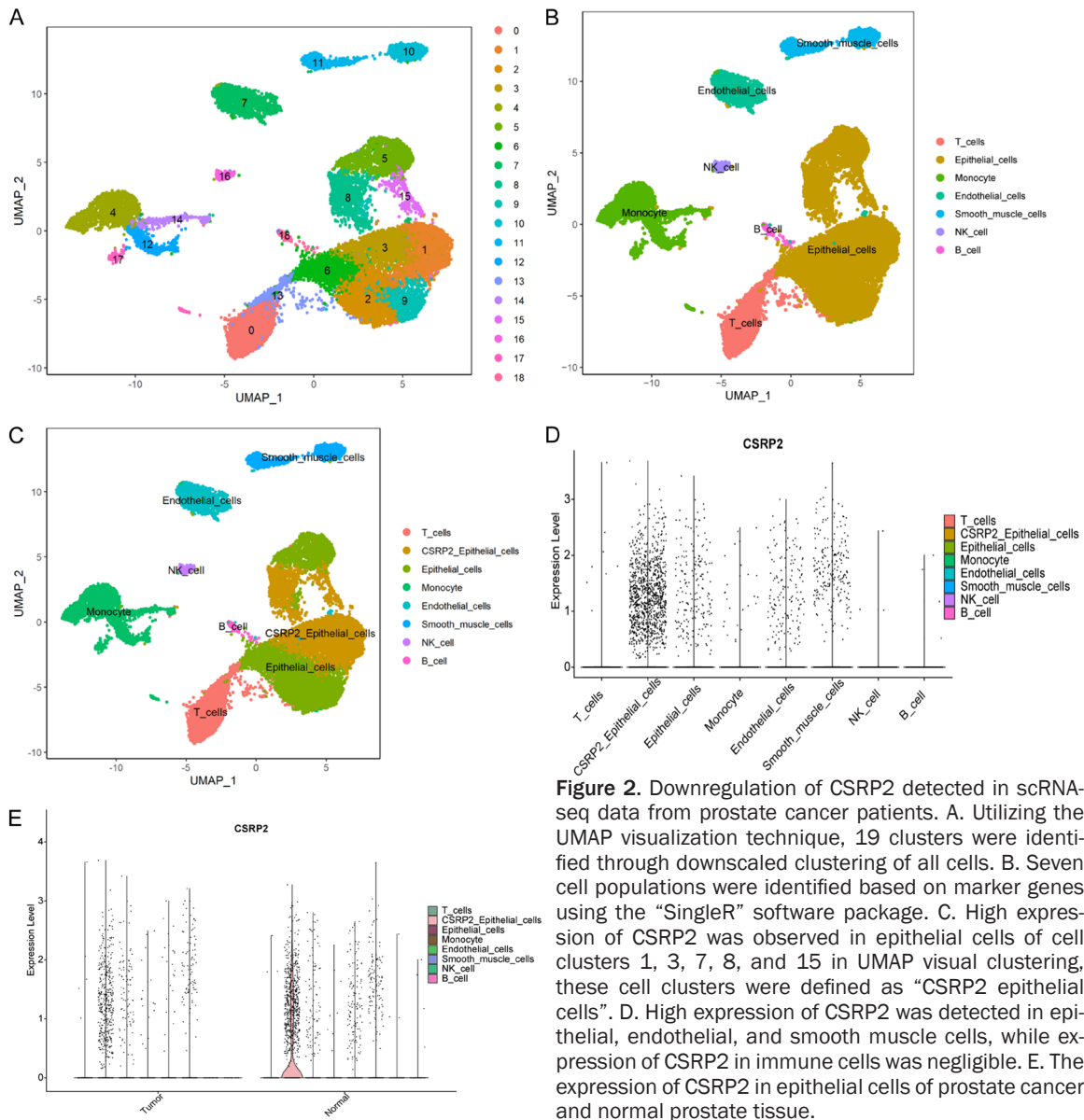
Figure 2. Downregulation of CSRP2 detected in scRNA-seq data from prostate cancer patients. A. Utilizing the UMAP visualization technique, 19 clusters were identified through downscaled clustering of all cells. B. Seven cell populations were identified based on marker genes using the "SingleR" software package. C. High expression of CSRP2 was observed in epithelial cells of cell clusters 1, 3, 7, 8, and 15 in UMAP visual clustering, these cell clusters were defined as "CSRP2 epithelial cells". D. High expression of CSRP2 was detected in epithelial, endothelial, and smooth muscle cells, while expression of CSRP2 in immune cells was negligible. E. The expression of CSRP2 in epithelial cells of prostate cancer and normal prostate tissue.

epithelial cells. Notably, *CSRP2*, *IGFBP5*, *SLC18A2*, *TMEFF2*, and *NIPAL35* were significantly upregulated in high CSRP2-expressing epithelial cells, while *AGR2*, *CD74*, *NEAT1*, *MT-ND4*, and *MALAT1* were significantly downregulated in these cells.

Further analysis using "irGSEA" revealed that the WNT-beta-catenin-signaling pathway was suppressed in high CSRP2-expressing epithelial cells, whereas unfolded-protein-response, TGF-beta-signaling, reactive-oxygen-species-pathway, protein-secretion, PI3K-AKT-mTOR signaling, and other pathways were significantly activated (Supplementary Figure 2D). Pseu-

dotemporal trajectory analysis indicated that high CSPR2-expressing epithelial cells were at an earlier stage of differentiation than low CSPR2-expressing epithelial cells (Supplementary Figure 2E-G).

The Branching Expression Analysis Model (BEAM) followed by hierarchical clustering analysis was used to better understand the gene expression profiles and potential cellular functions of epithelial cells over pseudotime. This approach identified four distinct gene expression modules, with the "cell fate 2" branching cell gene set primarily involved in humoral immune response, negative regulation of cell

population proliferation, apoptosis, and epithelial cell differentiation (Supplementary Figure 2H).

Knockdown of CSRP2 promotes proliferation of prostate cancer cells in vitro

To validate the findings described above, CSRP2 expression in prostate cancer cells was analyzed using immunofluorescence. The immunofluorescence results revealed lower expression of CSRP2 in cancer tissue than in adjacent paracancerous tissue (**Figure 3A**, **3B**), thus confirming the results presented above.

To obtain a more profound understanding of CSRP2 biology in the context of prostate cancer, cell proliferation (CCK-8), transwell, and colony formation assays were carried out using DU145 and PC3 prostate cancer cells with or without siRNA-mediated knockdown of CSRP2. Control experiments showed a substantial reduction in CSRP2 expression in prostate cancer cells treated with CSRP2-targeted siRNA (**Figure 3C**). The results of the CCK-8 assays demonstrated a time-dependent increase in cell proliferation in response to CSRP2 knockdown (**Figure 3D**). Consistent with this observation, the transwell and colony formation assays revealed more migrating cells and enhanced clonogenicity, respectively, in CSRP2 siRNA-treated cells than in control cells (**Figure 3E**, **3F**).

Overexpression of CSRP2 in vitro and in vivo inhibits prostate cancer progression

To test the idea that CSRP2 negatively regulates prostate carcinogenesis, DU145 and PC3 cells were transfected with pcDNA3.1-CSRP2. The results demonstrate reduced viability of prostate cancer cells that overexpress CSRP2 (**Figure 4A**). Moreover, prostate cancer cells overexpressing CSRP2 had reduced ability to form colonies and reduced capacity to migrate relative to control cells (**Figure 4B**, **4C**).

The role of CSRP2 in prostate cancer tumorigenesis was also examined using an *in vivo* xenograft assay in which tumor cells stably expressing pcDNA3.1-CSRP2 or empty vector (control) were injected into nude mice. The outcomes revealed that injected prostate cancer cells overexpressing CSRP2 grew more slowly than injected control cells (**Figure 4D**, n=5). Furthermore, immunofluorescence staining revealed a significant reduction in Ki67-positive cells, a marker of cell proliferation, in the CSRP2-overexpressing tumor cells of the injected mouse (**Figure 4E**). These results suggest that overexpression of CSRP2 inhibits the growth of prostate cancer cells *in vivo*.

CSRP2 inhibits deubiquitination of WDR5

The mechanism of action of CSRP2 was investigated by overexpressing Flag-tagged CSRP2 in PC3 cells while using GFP as a negative control. Proteins were immunoprecipitated using Flag magnetic beads and proteins subsequently released from the beads were analyzed by MS (**Figure 5A**). Six candidate CSRP2 binding proteins were identified and confirmed by carrying out three independent experiments. Notably, WDR5 was identified as a candidate CSRP2 binding protein and it ranked 5th in iBAQ value (**Figure 5B**). Data from the TCGA database indicated that overexpression of WDR5 in prostate cancer correlates with poor prognosis (**Figure 5C**), while other published studies also suggest that WDR5 is associated with prostate cancer progression [17, 18]. Thus, WDR5 is a strong candidate as a functionally important protein-interacting partner of CSRP2. The putative direct interaction between CSRP2 and WDR5 was investigated by carrying out a Co-IP assay, where Flag-tagged CSRP2 and GFP-tagged WDR5 were co-expressed (**Figure 5D**). Western blot analysis indicated that overexpression of CSRP2 in DU145 and PC3 cells led to a low level of WDR5 protein, implying that CSRP2 could alter the stability of WDR5 protein (**Figure 5E**). Consistent with this, when CSRP2-overexpressing cells were treated with cycloheximide (CHX), the half-life of WDR5 protein decreased (**Figure 5F**), while ubiquitination of WDR5 was higher in CSRP2 overexpressing cells. Notably, the ubiquitination of overexpressed CSRP2 was markedly enhanced when cells were treated with the proteasome inhibitor, MG132 (**Figure 5G**). Previous studies show that the deubiquitinating enzyme USP44 can prevent degradation of WDR5 [19]. Consistent with this, overexpression of CSPR2 in PC3 cells reduced binding of USP44 to WDR5, suggesting that the CSPR2-dependent effects on the stability of WDR5 are likely to be mediated by USP44 (**Figure 5H**).
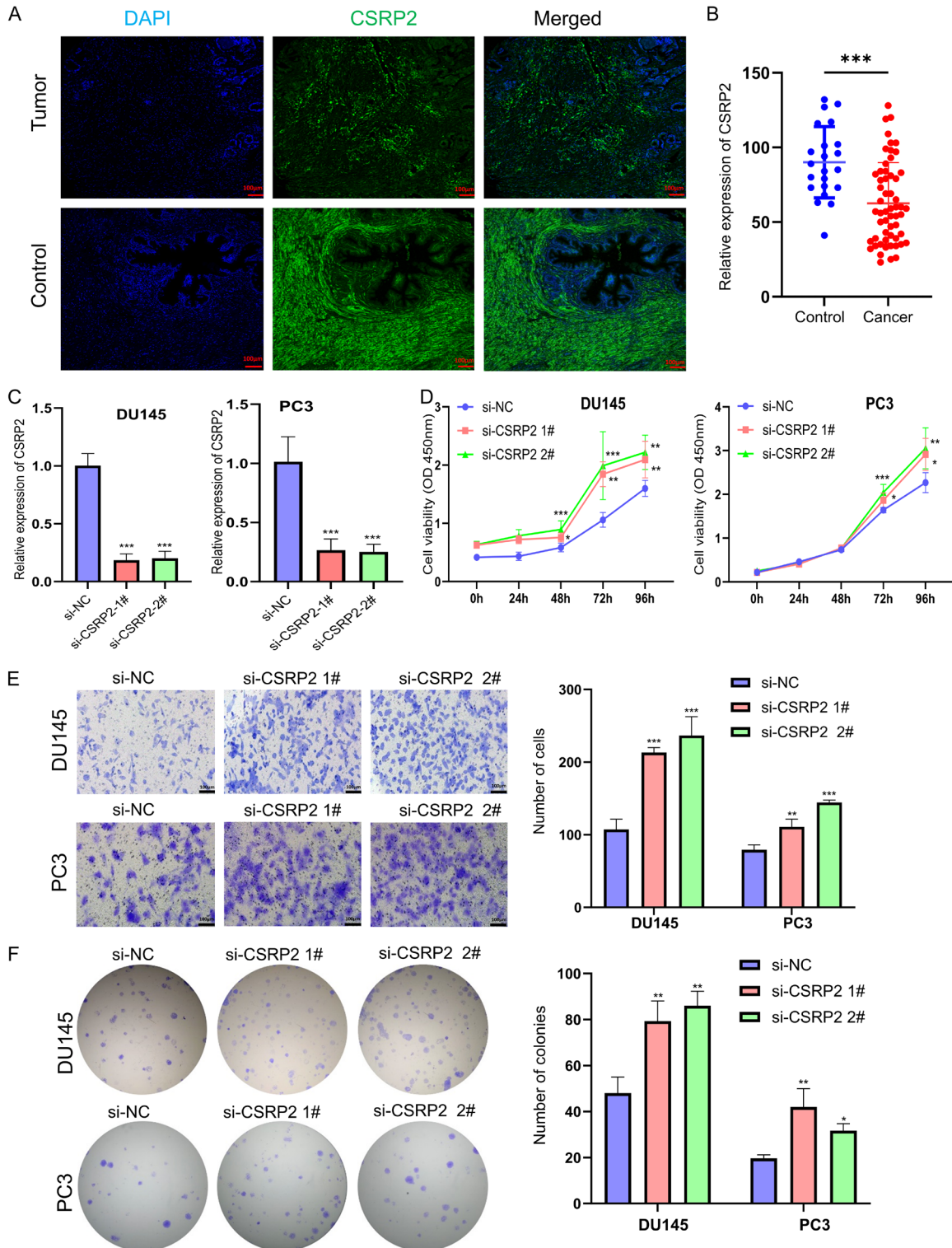
Figure 3. CSRP2 knockdown increases proliferation of prostate cancer cells *in vitro*. (A) Immunofluorescence detection of CSRP2 in prostate tissue. (B) Statistical data of Immunofluorescence. (C) Following transfection with si-CSRP2, a substantial reduction in CSRP2 expression was observed in the prostate cancer cell lines. (D) Cell proliferation increases over time after CSRP2 knockdown. (E, F) CSRP2 knockdown cells show greater capacity than control cells for colony formation and cell migration. $*P < 0.05$; $**P < 0.01$; $***P < 0.001$. All images in (A and E) were captured at 200× magnification, while in (F) were captured at 4× magnification.
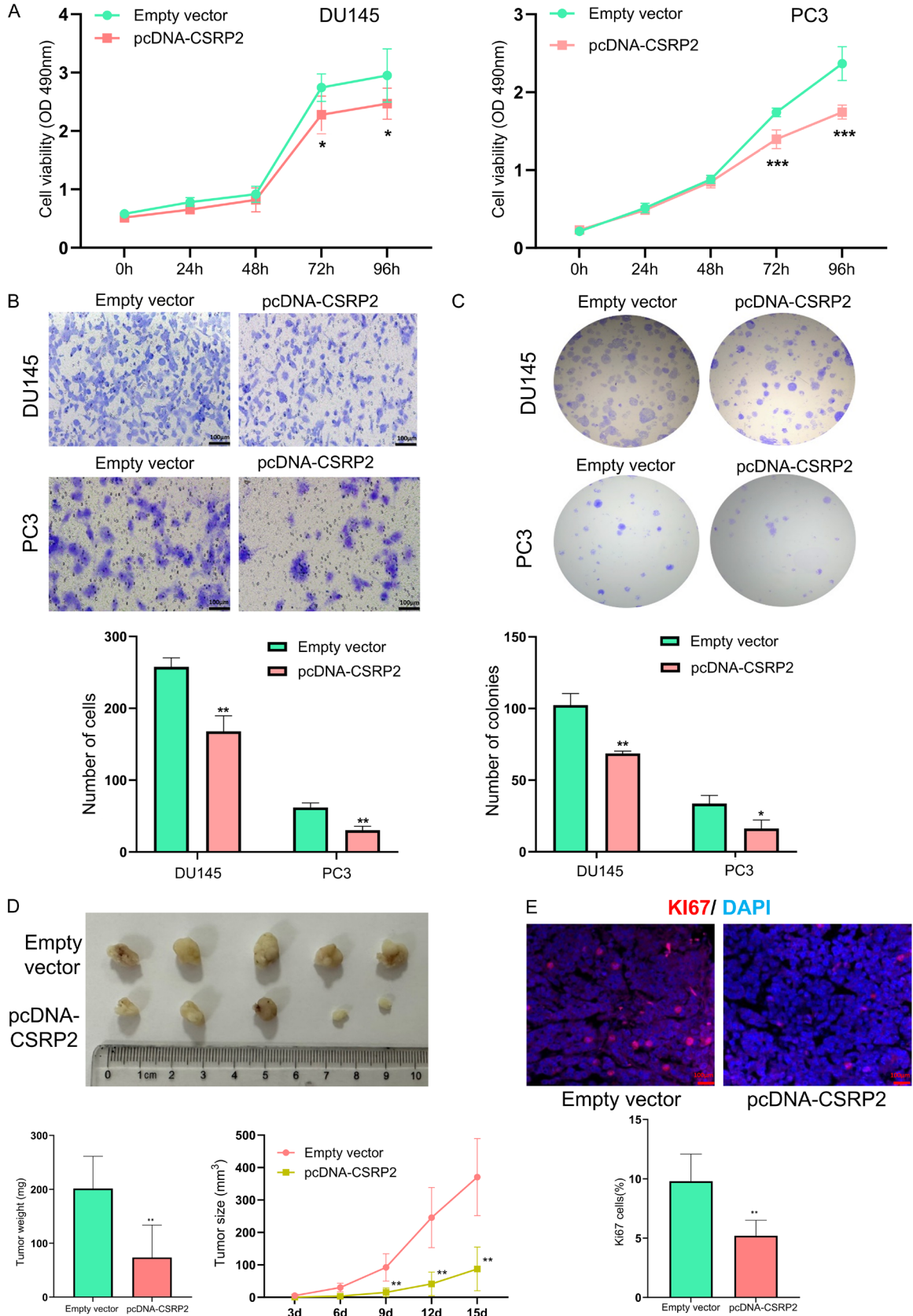
Figure 4. Effects of CSRP2 overexpression on prostate cancer cells *in vitro* and *in vivo*. (A) CCK-8 assays were performed to determine the cell viability of DU145 and PC3 cells transfected with pcDNA3.1-CSRP2. (B, C) Transwell

and colony forming assays were performed individually to investigate the changes in migratory abilities and cell viability of DU145 and PC3 cells overexpressing CSRP2. (D) Growth and proliferation of PC3 cells overexpressing of CSRP2 in nude mice. (E) Immunofluorescence and statistical results of proliferating cell nuclear antigen Ki67 expression in tumor formed by PC3 cells overexpressing CSRP2 injected into nude mice. n=5, *P < 0.05; **P < 0.01; ***P < 0.001. All images in (B and E) were captured at 200× magnification, while in (C) were captured at 4× magnification.

WDR5 overexpression reverses the effect of CSRP2 on prostate cancer cells

Considering that CSRP2 inhibits prostate cancer proliferation and migration and that it appears to interact directly with WDR5, we examined the effects of WDR5 overexpression and presumed activation of the WDR5 pathway on prostate cancer cells. The findings reveal that overexpression of WDR5 in CSRP2-overexpressed DU145 and PC3 cells substantially reversed the diminished cell proliferation (**Figure 6A**), modified colony formation (**Figure 6B**), and impeded cell migration caused by CSRP2 overexpression (**Figure 6C**).
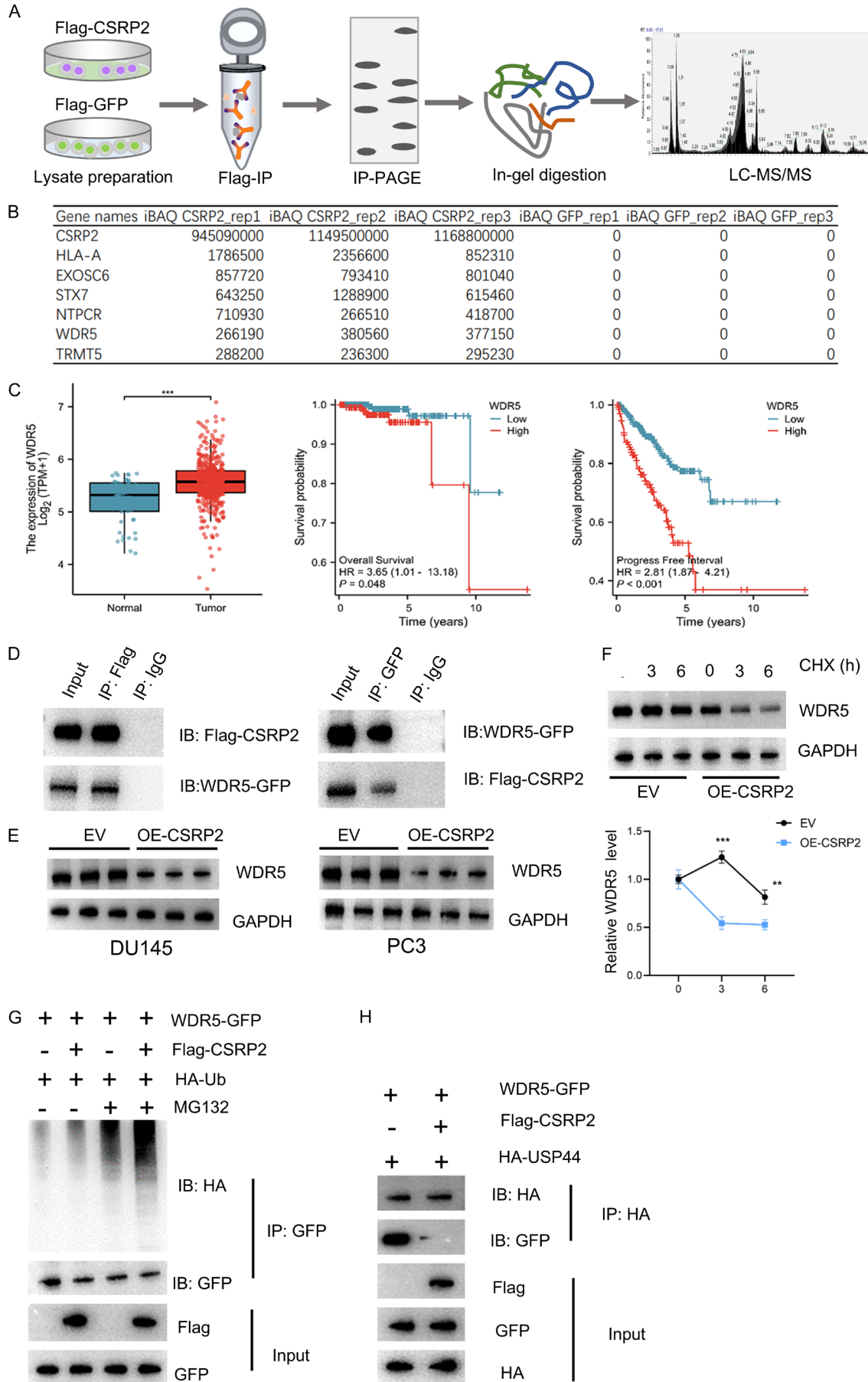
Discussion

Our data revealed that expression of CSRP2 was markedly downregulated in prostate cancer tissues, as evidenced by both scRNA-seq and bulk RNA-seq data, suggesting that CSRP2 may represent a novel oncogene. Both knockdown and overexpression of CSRP2 influenced the biological behavior of prostate cancer cells, underscoring its potential as a pivotal regulator of prostate cancer progression.

A LASSO regression analysis was conducted on 34 genes differentially expressed in subcutaneous adipose tissue and linked to OS from prostate cancer, resulting in the selection of 10 key genes - *TACC3, CCNL2, GPR35, CSRP2, PAQR6, E2F1, LY6G5B, SVOPL, NEK3,* and *DRD5* - which were used to develop a predictive model for prostate cancer risk. Prostate cancer patients were then stratified into high and low-risk groups based on their respective risk scores. The high-risk group exhibited a correlation with unfavorable prognosis, immune infiltration, immune escape, and chemotherapy response, underscoring the model's efficacy in both stratifying prostate cancer disease risk and predicting treatment responses. In particular, prostate cancer patients in the high-risk group were more sensitive to cisplatin but were insensitive to the androgen receptor blocker bicalutamide, both of which are used to treat prostate cancer. This discrepancy may be attributed to the significant enrichment of ubiquitin and ubiquitin-like protein ligase binding as revealed by GO analysis. In addition, GSVA uncovered substantial correlations between the high-risk group and processes such as base excision repair, homologous recombination, and DNA replication. Differential analysis of model genes using TCGA data revealed upregulation of *E2F1, PAQR6, NEK3, CCNL2,* and *TACC3* in prostate cancers, while the expression of *CSRP2* was downregulated. Specifically, upregulation of *PAQR6* in primary prostate cancer tissues emerged as a novel prognostic biomarker for disease progression, OS, and progression-free survival in prostate cancer [20]. Data on immune infiltration in prostate cancer tissue indicated that *CCNL2* could potentially serve as a novel biomarker for therapeutic decisions. The significantly lower methylation of *CCNL2* in tumor tissue was associated with its upregulation [21]. Notably, CSRP2 autoantibodies were more abundant in sera of prostate cancer patients following radical prostatectomy in hyperinflammatory cases [22]. Furthermore, CSRP2 was significantly downregulated in other sex-related tumors including BRCA, OV, and UCEC. Single-cell data analysis revealed higher expression of CSRP2 in epithelial, endothelial, and smooth muscle cells, but lower expression in immune cells. Additionally, expression of CSRP2 was markedly lower in cancer epithelial cells than in control epithelial cells. In summary, these observations suggest that CSRP2 is an important negative regulator of prostate cancer progression.

The CSRP2 protein includes two structural LIM domains and it exerts regulatory influence on cell growth, differentiation, and various oncogenic functions in multiple tumor types. In this study, we demonstrated that CSRP2 inhibits the proliferation, migration, and invasion of prostate cancer cells *in vitro* and that it impedes prostate cancer tumorigenesis and metastasis *in vivo*. IP-LC-MS/MS analysis revealed candidate CSRP2 binding proteins, with HLA-A rank-

CSRP2/WDR5/USP44 axis in prostate cancer progression

A

Flag-CSRP2 / Flag-GFP → Lysate preparation → Flag-IP → IP-PAGE → In-gel digestion → LC-MS/MS

B

Gene names	iBAQ CSRP2_rep1	iBAQ CSRP2_rep2	iBAQ CSRP2_rep3	iBAQ GFP_rep1	iBAQ GFP_rep2	iBAQ GFP_rep3
CSRP2	945090000	1149500000	1168800000	0	0	0
HLA-A	1786500	2356600	852310	0	0	0
EXOSC6	857720	793410	801040	0	0	0
STX7	643250	1288900	615460	0	0	0
NTPCR	710930	266510	418700	0	0	0
WDR5	266190	380560	377150	0	0	0
TRMT5	288200	236300	295230	0	0	0

Figure 5. The interaction between CSRP2 and WDR5 inhibits WDR5 deubiquitination by USP44. A. The IP-MS analysis flowchart. B. Putative CSRP2-interacting proteins and their respective iBAQ scores. C. Data from the TCGA database suggests that overexpression of WDR5 in prostate cancer is associated with a poor prognosis. D. Co-IP experiments reveal interactions between CSRP2 and WDR5. E. The effects of CSRP2 overexpression on WDR5 expressions in DU145 cells and PC3 cells. F. The effects of CHX treatment on the stability of WDR5 protein in PC3 cells. G. The effects of CSRP2 overexpression and protease inhibitor MG132 on WDR5 ubiquitination were measured by co-immunoprecipitation in PC3 cells. H. The effects of CSRP2 overexpression on the binding of USP44 to WDR5 were determined by co-immunoprecipitation in PC3 cells. **P < 0.01; ***P < 0.001.
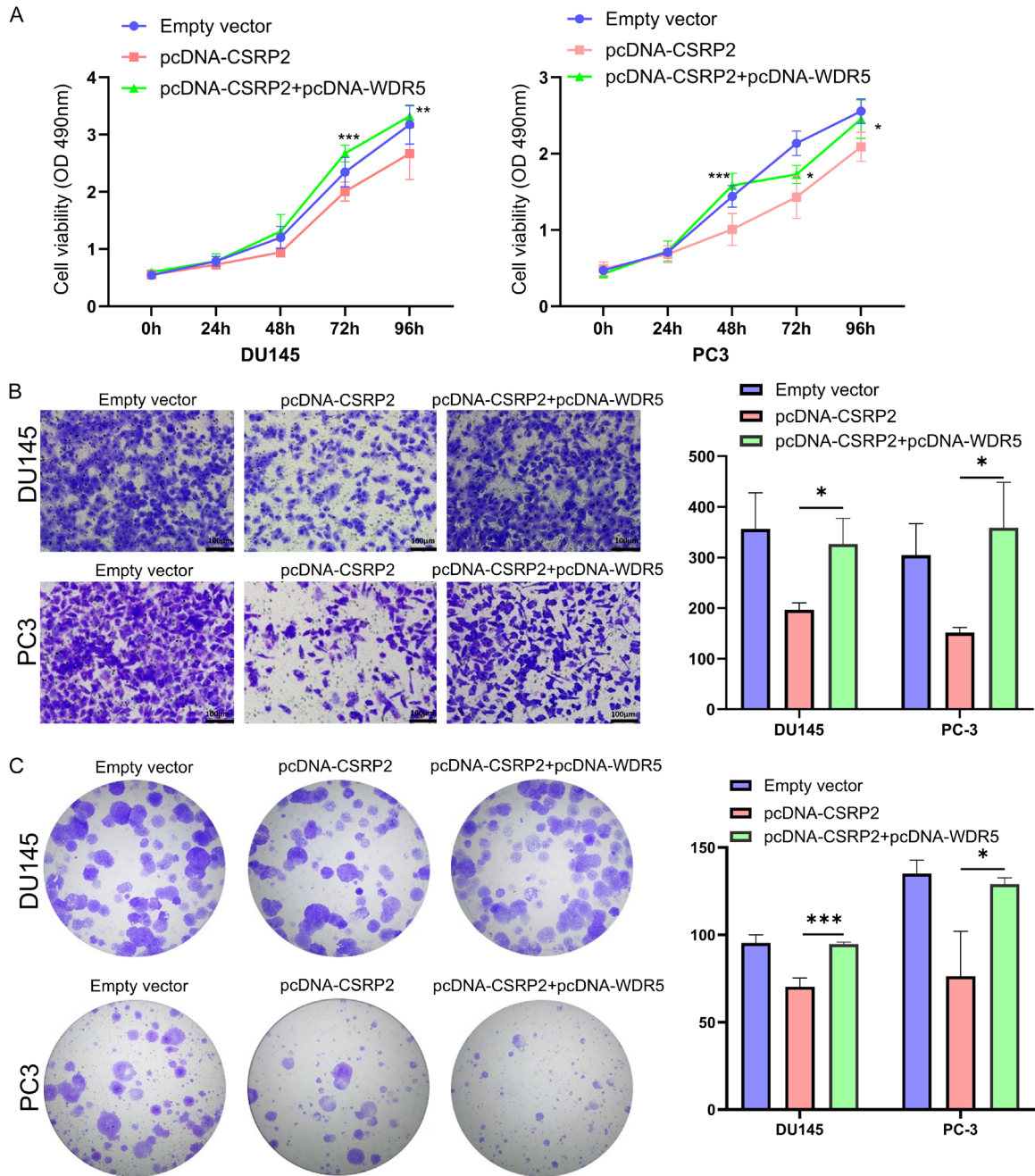

Figure 6. WDR5 overexpression reverses the effects of CSRP2 overexpression. Effects of WDR5 overexpression on the proliferation, clonality, and migration of prostate cancer cells overexpressing CSRP2. After transfection of DU145 and PC3 cells with EV (empty vector, control group), pcDNA-CSRP2 (overexpression of CSRP2) and pcDNA-CSRP2+pcDNA-WDR5 (overexpression of CSRP2 and WDR5), (A) the proliferation curve of CCK8 cells was shown, (B) transwell was used to detect cell migration, (C) Colony formation was observed by crystal violet staining. n=3, *P < 0.05, **P < 0.01, ***P < 0.001. All images in (B) were captured at 200× magnification, while in (C) were captured at 4× magnification.

ing first according to iBAQ. HLA-A is crucial for MHC class I molecules to present endogenous antigens, facilitating tumor immune escape when downregulated in prostate cancer [23]. Notably, WDR5 is a candidate protein-interacting partner of CSRP2, and previous studies have linked WDR5 to TWIST1 overexpression, which promotes prostate cancer metastasis [18].

Moreover, high expression of WDR5 in prostate cancers, as observed in TCGA data, correlates with poor prognosis. Our findings suggest that WDR5 may play a significant role in prostate cancer pathogenesis, potentially influenced by CSRP2. The results of Co-IP assays, cyclohexanamide (CHX) treatment, and ubiquitination assays suggest that CSRP2 inhibits cancer progression by binding to WDR5 and promoting its ubiquitination and subsequent degradation. Rescue experiments conclusively demonstrated that WDR5 overexpression reverses the effects of CSRP2 overexpression on the proliferation, migration, and colony-forming ability of prostate cancer cells. CSRP2-dependent degradation of WDR5 involves the ubiquitin-proteasome pathway, with a specific role for deubiquitinase USP44. In PC3 cells, overexpression of CSRP2 decreased binding of USP44 to WDR5, further confirming that the effect of CSRP2 on prostate cancer progression involves the interaction between CSRP2 and WDR5.

The effect of CSRP2 on tumor progression has also been reported in hematologic tumors and colorectal cancers. Wang et al. [24] identified that human CSRP2 transcript levels were upregulated in adults with B-cell ALL at the time of disease diagnosis, which was correlated with a higher cumulative incidence relapse. Focusing on colorectal cancer (CRC), Chen et al. [25] observed lower CSRP2 expression in cancer tissues than in paraneoplastic normal tissues. In CRC, CSRP2 inhibition suppresses the activation of Rac1, impedes the phosphorylation of p130Cas, and subsequently inhibits the Hippo signaling pathway, along with the ERK and PAK/LIMK/cortactin signaling pathways, leading to reduced proliferation, migration, and invasion of CRC cells. The different roles of CSRP2 in tumors may be due to the different origins of tumor cells; for instance, leukemia cells originate from blood cells and colorectal cancer cells originate from epithelial cells. Prostate cancer is also derived from epithelial cells, and our results are consistent with the study of CRC

reported by Chen et al. [25]. Therefore, CSRP2 may participate in the pathogenesis and progression of cancer originating from different cells through different mechanisms.

Recent investigations indicate that CSRP2 may contribute to tumor proliferation by affecting the epithelial-mesenchymal transition (EMT). Both *in vivo* and *in vitro* experiments show that the EMT plays an important role in the primary invasion and metastasis of prostate, colorectal, breast, lung, and other cancers. Wu et al. [26] found that WDR5 recruits the histone methyltransferase (HMT) complex to increase histone H3 lysine 4 (H3K4)-specific HMT activity and activate mesenchymal gene expression to promote EMT. Given that CSRP2 suppresses prostate cancer cell proliferation via a WDR5/USP44-dependent pathway, we hypothesize that the EMT may be a vital molecular mechanism by which CSRP2 participates in prostate cancer progression. We plan to study this hypothesis further in the future.

In conclusion, this study reports a newly developed model for predicting prognosis, immune cell infiltration, and chemotherapy response in prostate cancer. The model is based on CSRP2 and nine other marker genes that are differentially expressed in subcutaneous adipose tissue. CSRP2 expression is a key determinant of prostate cancer risk that is markedly downregulated in subcutaneous adipose tissue, interacts with WDR5, and regulates WDR5 protein stability by a mechanism involving USP44.

Acknowledgements

Disclosure of conflict of interest

The authors declare that the research was conducted in the absence of any commercial or financial relationships that could be construed as a potential conflict of interest.

Address correspondence to: Li Li, Department of Laboratory Medicine, Shanghai General Hospital, Shanghai Jiao Tong University School of Medicine,

No. 85 Wujin Road, Hongkou District, Shanghai 200080, China. E-mail: annylish@126.com; Longwei Qiao, State Key Laboratory of Reproductive Medicine, Center for Reproduction and Genetics, School of Gusu, The Affiliated Suzhou Hospital of Nanjing Medical University, Suzhou Municipal Hospital, Nanjing Medical University, No. 26 Daoqian Street, Suzhou 215002, Jiangsu, China. E-mail: qiaolongwei1@126.com; Jia Li, Medical Laboratory, Shidong Hospital Affiliated to University of Shanghai for Science and Technology, No. 999 Shiguang Road, Yangpu District, Shanghai 200438, China. E-mail: 1124lijia@163.com
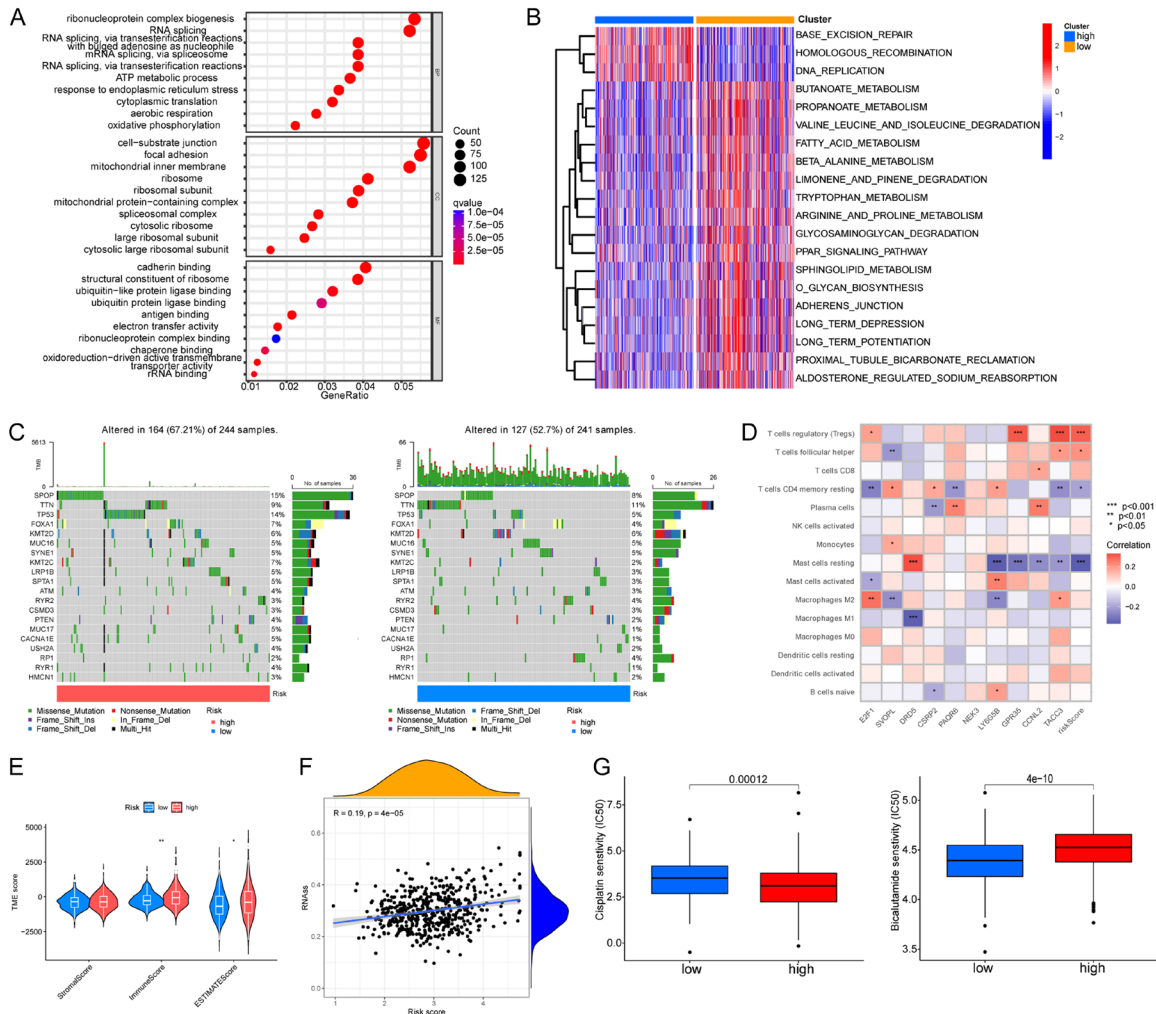
References

[1] Siegel RL, Miller KD, Fuchs HE and Jemal A. Cancer statistics, 2022. CA Cancer J Clin 2022; 72: 7-33.

[2] Siegel RL, Miller KD and Jemal A. Cancer statistics, 2018. CA Cancer J Clin 2018; 68: 7-30.

[3] Rebello RJ, Oing C, Knudsen KE, Loeb S, Johnson DC, Reiter RE, Gillessen S, Van der Kwast T and Bristow RG. Prostate cancer. Nat Rev Dis Primers 2021; 7: 9.

[4] Berish RB, Ali AN, Telmer PG, Ronald JA and Leong HS. Translational models of prostate cancer bone metastasis. Nat Rev Urol 2018; 15: 403-421.

[5] Wasim S, Lee SY and Kim J. Complexities of prostate cancer. Int J Mol Sci 2022; 23: 14257.

[6] Boyd LK, Mao X and Lu YJ. The complexity of prostate cancer: genomic alterations and heterogeneity. Nat Rev Urol 2012; 9: 652-664.

[7] Martinez-Jimenez F, Movasati A, Brunner SR, Nguyen L, Priestley P, Cuppen E and Van Hoeck A. Pan-cancer whole-genome comparison of primary and metastatic solid tumours. Nature 2023; 618: 333-341.

[8] Zhong W, Wang X, Wang Y, Sun G, Zhang J and Li Z. Obesity and endocrine-related cancer: the important role of IGF-1. Front Endocrinol (Lausanne) 2023; 14: 1093257.

[9] Choi JB, Myong JP, Lee Y, Kim I, Kim JH, Hong SH and Ha US. Does increased body mass index lead to elevated prostate cancer risk? It depends on waist circumference. BMC Cancer 2020; 20: 589.

[10] Miladinovic D, Cusick T, Mahon KL, Haynes AM, Cortie CH, Meyer BJ, Stricker PD, Wittert GA, Butler LM, Horvath LG and Hoy AJ. Assessment of periprostatic and subcutaneous adipose tissue lipolysis and adipocyte size from men with localized prostate cancer. Cancers (Basel) 2020; 12: 1385.

[11] Delouya G, Tiberi D, Bhatnagar SR, Campeau S, Saad F and Taussky D. Impact of adipose tissue on prostate cancer aggressiveness - analysis of a high-risk population. Horm Mol Biol Clin Investig 2018; 36.

[12] Vertulli D, Santucci D, Esperto F, Beomonte Zobel B, Grasso RF and Faiella E. Impact of adipose tissue distribution on prostate cancer recurrence after radical prostatectomy. Actas Urol Esp (Engl Ed) 2023; 47: 104-110.

[13] Hu X, Hu C, Zhang C, Zhang M, Long S and Cao Z. Role of adiponectin in prostate cancer. Int Braz J Urol 2019; 45: 220-228.

[14] Wang S, Wang N, Yu B, Cao M, Wang Y, Guo Y, Zhang Y, Zhang P, Yu X, Wang S, Zeng L, Liang B, Li X and Wu Y. Circulating IGF-1 promotes prostate adenocarcinoma via FOXO3A/BIM signaling in a double-transgenic mouse model. Oncogene 2019; 38: 6338-6353.

[15] Klimcakova E, Roussel B, Marquez-Quinones A, Kovacova Z, Kovacikova M, Combes M, Siklova-Vitkova M, Hejnova J, Sramkova P, Bouloumie A, Viguerie N, Stich V and Langin D. Worsening of obesity and metabolic status yields similar molecular adaptations in human subcutaneous and visceral adipose tissue: decreased metabolism and increased immune response. J Clin Endocrinol Metab 2011; 96: E73-82.

[16] Song H, Weinstein HNW, Allegakoen P, Wadsworth MH 2nd, Xie J, Yang H, Castro EA, Lu KL, Stohr BA, Feng FY, Carroll PR, Wang B, Cooperberg MR, Shalek AK and Huang FW. Single-cell analysis of human primary prostate cancer reveals the heterogeneity of tumor-associated epithelial cell states. Nat Commun 2022; 13: 141.

[17] Kim JY, Banerjee T, Vinckevicius A, Luo Q, Parker JB, Baker MR, Radhakrishnan I, Wei JJ, Barish GD and Chakravarti D. A role for WDR5 in integrating threonine 11 phosphorylation to lysine 4 methylation on histone H3 during androgen signaling and in prostate cancer. Mol Cell 2014; 54: 613-625.

[18] Malek R, Gajula RP, Williams RD, Nghiem B, Simons BW, Nugent K, Wang H, Taparra K, Lemtiri-Chlieh G, Yoon AR, True L, An SS, DeWeese TL, Ross AE, Schaeffer EM, Pienta KJ, Hurley PJ, Morrissey C and Tran PT. TWIST1-WDR5-Hottip regulates Hoxa9 chromatin to facilitate prostate cancer metastasis. Cancer Res 2017; 77: 3181-3193.

[19] Chi Z, Zhang B, Sun R, Wang Y, Zhang L and Xu G. USP44 accelerates the growth of T-cell acute lymphoblastic leukemia through interacting with WDR5 and repressing its ubiquitination. Int J Med Sci 2022; 19: 2022-2032.

[20] Yang M, Li JC, Tao C, Wu S, Liu B, Shu Q, Li B and Zhu R. PAQR6 upregulation is associated with AR signaling and unfavorite prognosis in prostate cancers. Biomolecules 2021; 11: 1383.

[21] Li Q, Chen B, Song G, Zeng K, Chen X, Miao J, Yuan X, Liu J, Wang Z and Liu B. Integrated analysis to identify the AC005154.6/hsa-miR-29c-3p/CCNL2 axis as a novel prognostic biomarker associated with immune infiltration in prostate cancer. Cancer Cell Int 2022; 22: 346.

[22] Schlick B, Massoner P, Lueking A, Charoentong P, Blattner M, Schaefer G, Marquart K, Theek C, Amersdorfer P, Zielinski D, Kirchner M, Trajanoski Z, Rubin MA, Mullner S, Schulz-Knappe P and Klocker H. Serum autoantibodies in chronic prostate inflammation in prostate cancer patients. PLoS One 2016; 11: e0147739.

[23] Manca MA, Simula ER, Cossu D, Solinas T, Madonia M, Cusano R and Sechi LA. Association of HLA-A*11:01, -A*24:02, and -B*18:01 with prostate cancer risk: a case-control study. Int J Mol Sci 2023; 24: 15398.

[24] Wang SJ, Wang PZ, Gale RP, Qin YZ, Liu YR, Lai YY, Jiang H, Jiang Q, Zhang XH, Jiang B, Xu LP, Huang XJ, Liu KY and Ruan GR. Cysteine and glycine-rich protein 2 (CSRP2) transcript levels correlate with leukemia relapse and leukemia-free survival in adults with B-cell acute lymphoblastic leukemia and normal cytogenetics. Oncotarget 2017; 8: 35984-36000.

[25] Chen L, Long X, Duan S, Liu X, Chen J, Lan J, Liu X, Huang W, Geng J and Zhou J. CSRP2 suppresses colorectal cancer progression via p130Cas/Rac1 axis-meditated ERK, PAK, and HIPPO signaling pathways. Theranostics 2020; 10: 11063-11079.

[26] Wu MZ, Tsai YP, Yang MH, Huang CH, Chang SY, Chang CC, Teng SC and Wu KJ. Interplay between HDAC3 and WDR5 is essential for hypoxia-induced epithelial-mesenchymal transition. Mol Cell 2011; 43: 811-822.

Supplementary Figure 1. The predictive model is associated with immune cell infiltration and chemotherapy in prostate cancer. A. GO analysis describes the differences between high-risk and low-risk groups. B. The GSVA of KEGG pathways reveals enrichment of different signaling pathways in each risk group. C. The mutational landscape of prostate cancer cells in high- and low-risk groups. D. The correlation between immune infiltration, 10 marker genes, and risk scores is shown. E. The immune score and ESTIMATE score in the TME score are significantly higher in the high-risk group. F. The correlation between risk score and tumor stemness was quantified by RNAss. G. The association between risk score and response to chemotherapy targeting prostate cancer.

Supplementary Figure 2. Functions and pathways associated with high expression of CSRP2 in epithelial cells. A. Genes characteristic of cellular subpopulations are shown. B, C. The proportion of epithelial cells exhibiting high levels of CSRP2 in normal tissue and prostate cancer. D. Relationship between CSRP2 expression and cell function. E-G. Pseudotemporal trajectory analysis of epithelial cells with high levels of CSRP2 and their stage of differentiation. H. BEAM analysis of gene expression profiles and putative functional roles of epithelial cell subpopulations over pseudotime.